

Quantum interferometry for rotation sensing in an optical microresonator

Weijun Cheng,¹ Zhihai Wang,^{1,*} and Xiaoguang Wang^{2,†}

¹Center for Quantum Sciences and School of Physics, Northeast Normal University, Changchun 130024, China

²Zhejiang Institute of Modern Physics, Department of Physics, Zhejiang University, Hangzhou 310027, China



(Received 4 November 2021; accepted 7 February 2022; published 22 February 2022)

We theoretically propose a scheme to perform rotation sensing in a whispering-gallery-mode resonator setup. With the assistance of a largely detuned two-level atom, which induces the effective coupling between clockwise- and counterclockwise-propagating modes in the resonator, we realize an effective interferometry with SU(2) algebraic structure. By studying the quantum Fisher information of the system, we find that the estimated accuracy for the angular velocity of the rotation can achieve and even break the Heisenberg limit in the linear and nonlinear setup, respectively. The high performance of quantum metrology is proved to be associated with the state compressibility during the time evolution. We hope that our investigation will be useful in the design of a quantum gyroscope based on spinning resonators.

DOI: [10.1103/PhysRevA.105.023716](https://doi.org/10.1103/PhysRevA.105.023716)

I. INTRODUCTION

The ultraprecise estimation of parameters, which was introduced in quantum interferometry [1,2], has been widely promoted to be the optical microresonator. The theory claims that the quantum features such as entanglement and squeeze can dramatically enhance the interferometer sensitivity [3–6]. In this community, the phase sensitivity of the interferometer can approach the Heisenberg limit with $\Delta x \sim 1/n$ (n is the amount of the source employed) scaling, which is much better than the classical astrict, named the standard quantum limit with $\Delta x \sim 1/\sqrt{n}$ scaling.

Quantum interferometry is achieved by measuring the intensity difference at the output of the interferometer [7–10]. Typically, the sensitivity enhancements in different types of interferometric schemes have been proposed in many setups, such as Sagnac, Mach-Zehnder, Fabry-Pérot, and SU(1,1) interferometers [11–20]. Nowadays, instead of exploring quantum metrology in the interferometer, quantum sensors composed by, for example, quantum dot and cavity QED systems, have made great achievements [21–31]. As one kind of the simple two-mode resonant cavities, the whispering-gallery-mode (WGM) resonator has become a versatile platform for measuring the angular velocity based on the Sagnac effect [32,33].

The WGM supports the clockwise and counterclockwise propagating optical modes, and the effective coupling between the two optical modes can be induced by coupling to a largely detuned two-level atom. Adiabatically eliminating the degree of freedom of the atom, we construct an effective interferometer with SU(2) Lie algebra structure in this paper. It is thus similar to the Mach-Zehnder interferometer and supplies us a way to perform the rotating sensing. The underlying physics is to transform the information about the angular velocity to the phase difference of the two optical

modes. The study about the quantum Fisher information (QFI) shows that the effective intermode coupling, which encodes the information of rotation into both of the amplitudes and the phases of the wave function, plays a decisive role in achieving the Heisenberg limit for the estimation of angular velocity. Moreover, we find that even a weak nonlinearity in the system will further enhance the quantum metrology and defeat the Heisenberg limit by achieving a $1/n^3$ scaling for the QFI. We explain the enhancement by the compressibility of state distribution during the time evolution.

The rest of the paper is organized as follows. In Sec. II, we review quantum interferometry and present a feasible experimental scheme in the WGM optical microresonator. In Sec. III, we discuss the effect of the nonlinearity in the system for enhancing the quantum metrology. In Sec. IV, we give a short summary. In the Appendixes, we present some detailed calculations.

II. MODEL AND HAMILTONIAN

A. Mach-Zehnder interferometer

Let us first review the Mach-Zehnder interferometer, which is sketched in Fig. 1(a). It consists of two 50:50 beam splitters S_1 and S_2 , the relative phase shift device $\phi = \phi_2 - \phi_1$, and the photodetectors D_1 and D_2 . It is convenient to introduce the Schwinger representation for a two-mode quantized light field, that is,

$$\begin{aligned} J_x &= \frac{1}{2}(ab^\dagger + a^\dagger b), \\ J_y &= \frac{1}{2i}(ab^\dagger - a^\dagger b), \\ J_z &= \frac{1}{2}(a^\dagger a - b^\dagger b), \\ J^2 &= J_x^2 + J_y^2 + J_z^2, \end{aligned} \quad (1)$$

and

$$N = a^\dagger a + b^\dagger b. \quad (2)$$

*wangzh761@nenu.edu.cn

†xgwang1208@zju.edu.cn

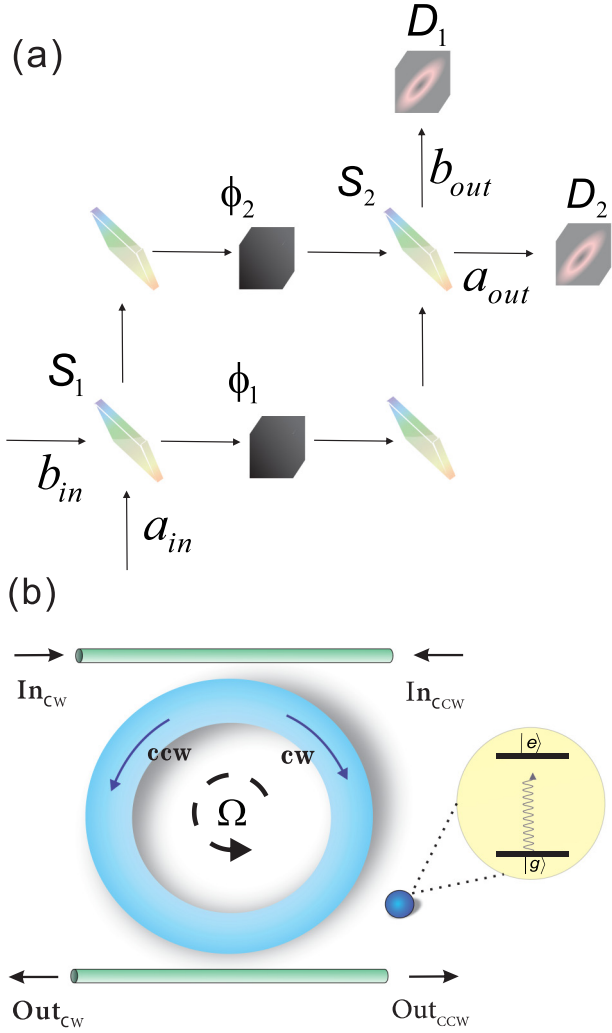


FIG. 1. (a) Schematic diagram of the Mach-Zehnder interferometer. It consists of two 50:50 beam splitters S_1 and S_2 , the relative phase shift device $\phi = \phi_2 - \phi_1$, and the photodetectors D_1 and D_2 . (b) Sketch of a rotating whispering-gallery-mode optical resonator, which couples to a largely detuned two-level atom.

Here a and b represent the annihilation operation of two beams and the commutation relations satisfy the Lie algebra of $SU(2)$:

$$[J_x, J_y] = iJ_z, [J_y, J_z] = iJ_x, [J_z, J_x] = iJ_y. \quad (3)$$

It then yields

$$\begin{aligned} J_z |j, m\rangle &= m |j, m\rangle, \\ J^2 |j, m\rangle &= j(j+1) |j, m\rangle, \end{aligned} \quad (4)$$

and

$$N |j, m\rangle = n |j, m\rangle, \quad (5)$$

where $n = 2j$ is the total number of photons and m is the difference of photon number between the two ports.

For the sake of convenience, here and after, we set the entangled initial state as $|\text{in}\rangle = (|j, 0\rangle + |j, 1\rangle)/\sqrt{2}$. In the Schrödinger picture, the devices S_1 , S_2 , and $\phi = \phi_2 - \phi_1$ will lead to transformations $\exp(-i\pi J_x/2)$, $\exp(i\pi J_x/2)$, and

$\exp(-i\phi J_z)$, respectively. The final state $|\text{out}\rangle$ is thus

$$|\text{out}\rangle = U(\phi)|\text{in}\rangle = e^{i\frac{\pi}{2}J_x} e^{-i\phi J_z} e^{-i\frac{\pi}{2}J_x} |\text{in}\rangle. \quad (6)$$

As an interferometer, the phase difference ϕ is the parameter to be estimated. In the field of quantum metrology, the QFI is a central quantity, giving a theoretically achievable limit on the precision for an unknown estimated parameter ϕ . Considering the parameter ϕ as a random variable the mean-square fluctuation of ϕ is defined as $\Delta\phi = \sqrt{\overline{\phi^2} - \bar{\phi}^2}$. According to the quantum Cramér-Rao inequality, $\Delta\phi$ is bounded by [34–37]

$$\Delta\phi \geq \frac{1}{\sqrt{\nu \mathcal{F}_\phi}}, \quad (7)$$

where ν are the times of the independent measurements and \mathcal{F}_ϕ is the QFI with respect to ϕ . For a general quantum pure state $|\psi\rangle$, the QFI is given by

$$\mathcal{F}_\phi = 4(\langle \partial_\phi \psi | \partial_\phi \psi \rangle - |\langle \psi | \partial_\phi \psi \rangle|^2). \quad (8)$$

Introducing a Hermitian operator

$$\mathcal{H} = -iU^\dagger (\partial U / \partial \phi) \quad (9)$$

(U is the evolution operation), the QFI can be reduced to

$$\mathcal{F}_\phi = 4\langle \Delta^2 \mathcal{H} \rangle, \quad (10)$$

where $\Delta^2 \mathcal{H} = \langle \mathcal{H}^2 \rangle - \langle \mathcal{H} \rangle^2$.

Then we have

$$\mathcal{F}_\phi = 2j(j+1) - 1, \quad (11)$$

so that $\Delta\phi \simeq \sqrt{2}/n$, that is, the fluctuation of ϕ is proportional to $1/n$, which is referred to as the Heisenberg limit. Furthermore, we note that the QFI will decline dramatically to 1 without the 50:50 beam splitters. In fact, the 50:50 beam splitters, whose roles are described by $e^{\pm i(\pi/2)J_x}$ in Eq. (6), will induce the effective coupling between the a and b modes and therefore improve measurement accuracy.

B. Cavity QED setup

In the above subsection, we exhibited the effect of the Mach-Zehnder interferometer in regard to achieving the Heisenberg limit for the phase estimating. In this subsection, mimicking the parametric process in the Mach-Zehnder interferometer, we design the quantum sensors for rotation in a WGM optical microresonator. The central idea is that the information of the angular velocity of the rotation is transferred to the effective phase between the two ports.

As one of the most simple two-mode resonant cavity, the WGM optical microresonator shows excellent performance in measuring the angular velocity [38,39], and the similar Sagnac-effect-based rotation rate sensitivity is reported to be with sub-prad/s [33], which is even beyond the Earth's rotation rate (7.292×10^{-5} rad/s). We now apply the optical microresonator, which couples to a two-level largely detuned atom to perform a quantum sensing as illustrated in Fig. 1(b). Here, the atom with energy separation ω_a between the ground state $|g\rangle$ and excited state $|e\rangle$ is placed near the resonator with an optical resonance frequency ω_l . The optical microresonator supports two resonant modes, which are propagated clockwise

(CW) and counterclockwise (CCW), and as shown below, the two-level atom will induce a weak effective interaction between the two modes. Furthermore, we introduce two parallel waveguides, which couple to the microresonator. The waveguides can be applied to prepare the input state and perform the measurement on the output photons of the CW and CCW modes as shown in Fig. 1(b) [40].

We consider a gyro setup where the waveguides are stationary while the microresonator is rotated with angular velocity Ω . Such a spinning resonator was realized experimentally and demonstrate the photonic nonreciprocal transmission [41]. Thanks to the rotation, the optical resonance frequency will be modified $\omega_l \rightarrow \omega_l \pm \Delta$ due to the Sagnac effect [42], where

$$\Delta = \frac{n_0 R \Omega \omega_l}{c} \left(1 - \frac{1}{n_0^2} - \frac{\lambda}{n_0} \frac{dn_0}{d\lambda} \right). \quad (12)$$

Here n_0 is the refractive index, R is the radius of resonator, and c is the speed of light in a vacuum. λ is the wavelength of the probe light and the last term $\lambda dn_0/n_0 d\lambda$ originates from the relativistic effect. The Hamiltonian of the system can be written as $H = H_0 + H_I$, where

$$H_0 = \sum_{\gamma} \omega_{\gamma} a_{\gamma}^{\dagger} a_{\gamma} + \omega_a |e\rangle\langle e|, \quad (13)$$

and

$$H_I = \sum_{\gamma} (g_{\gamma} a_{\gamma} |e\rangle\langle g| + \text{H.c.}). \quad (14)$$

Here, $\gamma = \text{cw, ccw}$, and $\omega_{\text{cw}} = \omega_l + \Delta$, $\omega_{\text{ccw}} = \omega_l - \Delta$. The real g_{γ} is the coupling strength between the γ mode and the two-level atom. a_{γ} and a_{γ}^{\dagger} are the annihilation and creation operators of the γ mode, respectively. By use of the Frölich-Nakajima transformation (see Appendix A) and the Schwinger representation, the approximate effective Hamiltonian of the system can be reduced to

$$\tilde{H}_{\text{eff}} = f(\Delta) J_z + d J_x, \quad (15)$$

where $f = 2\Delta$ and $d = 2g_{\text{eff}}$. Here, the effective coupling strength between the two optical modes g_{eff} is (refer to Appendix A for detailed derivations)

$$g_{\text{eff}} = \frac{1}{2} \left(\frac{1}{\Delta_{\text{cw}}} + \frac{1}{\Delta_{\text{ccw}}} \right) g_{\text{cw}} g_{\text{ccw}}, \quad (16)$$

with $\Delta_{\gamma} = \omega_a - \omega_{\gamma}$ ($\gamma = \text{CW, CCW}$). g_{eff} implies that the photon in CW (CCW) mode is virtually absorbed by the atom, and remitted it to the CCW (CW) mode, therefore, the two modes couple to each other via a second-order process.

Similar to the Mach-Zehnder interferometer, the parametric process is governed by the evolution $U = \exp(-i\tilde{H}_{\text{eff}}t)$. We would like to emphasize that the roll of the beam splitters is replaced by the atom, which induces the effective coupling between the two modes and d in Eq. (15) characterizes the coupling strength.

To calculate the QFI with respect to Δ , we give directly the Hermitian operator in Eq. (9) as [43,44]

$$\mathcal{H}_{\text{eff}} = C_x J_x + C_y J_y + C_z J_z, \quad (17)$$

where

$$\begin{aligned} C_x &= \frac{df}{r^3} \frac{\partial f}{\partial \Delta} [\sin(rt) - rt], \\ C_y &= \frac{d}{r^2} \frac{\partial f}{\partial \Delta} [\cos(rt) - 1], \\ C_z &= -\frac{d^2}{r^3} \frac{\partial f}{\partial \Delta} \left[\sin(rt) + \frac{f^2 rt}{d^2} \right], \end{aligned} \quad (18)$$

and $r = \sqrt{f^2 + d^2}$. Thus

$$\begin{aligned} \mathcal{F}_{\phi} &= \left[\frac{n}{2} \left(\frac{n}{2} + 1 \right) - 1 \right] C_x^2 \\ &\quad + 2 \left[\frac{n}{2} \left(\frac{n}{2} + 1 \right) - \frac{1}{2} \right] C_y^2 + C_z^2. \end{aligned} \quad (19)$$

Obviously, we have $\mathcal{F}_{\phi} \sim n^2$, which achieves the Heisenberg limit. However, when $d = 0$, it will become $\mathcal{F}_{\phi} = (\partial f / \partial \Delta) t^2$, which is independent of n and is smaller than that for $d \neq 0$. It indicates that the effective coupling between two modes, which is induced by the largely detuned atom, plays a pivotal role for enhancing quantum metrology and achieving the Heisenberg limit.

The enhancement of QFI originates from the special encoding scheme for a quantum state. Without intermode coupling (i.e., $d = 0$), the information about Δ is only encoded in the phase of the quantum state. However, the atom-induced coupling makes not only the phase but also the amplitude contain the information about rotation (Δ). As derived in Appendix B, we will get an enhancement for QFI. Specifically, when $d = 0$, the dynamical evolution is obtained by $|\psi(t)\rangle = \exp(-i(fJ_z t)|\text{in}) = (|j, 0\rangle + \exp(-ift)|j, 1\rangle) / \sqrt{2}$ and thus Δ is only encoded in the phase. However, for $d \neq 0$, the evolution will become complicated: $|\psi(t)\rangle = \exp[-i(fJ_z + dJ_x)t]|\text{in})$. Under this circumstance, the information of Δ is not only carried in the phase, but also in the probability amplitude, leading to an enhancement of the quantum metrology.

III. NONLINEAR EFFECT

In the above section, we outlined that the effective coupling between the CW and CCW modes, which is induced by the two-level atom, plays a vital role in achieving the Heisenberg limit. To further improve the measurement accuracy, we consider an extra nonlinear term in this section.

For the general nonlinear microcavity system, the Kerr type is one of the most common forms, which is hosted in a cavity that is filled by the atoms with a particular laser-driving four-level structure [45,46]. Combining the above linear model, the current system can be described by the Bose-Hubbard Hamiltonian

$$\begin{aligned} H &= \sum_{\gamma} \{ \omega_{\gamma} a_{\gamma}^{\dagger} a_{\gamma} + U (a_{\gamma}^{\dagger} a_{\gamma} a_{\gamma}^{\dagger} a_{\gamma} - a_{\gamma}^{\dagger} a_{\gamma}) \} \\ &\quad + g_{\text{eff}} (a_{\text{cw}}^{\dagger} a_{\text{ccw}} + a_{\text{ccw}}^{\dagger} a_{\text{cw}}), \end{aligned} \quad (20)$$

where U is the on-side interaction strength and $\gamma = \text{cw, ccw}$. In the Schwinger representation, it can be reduced to

$$\begin{aligned} H &= (\omega_l + U)N + \frac{U}{2}N^2 + 2UJ_z^2 \\ &\quad + 2\Delta J_z + 2g_{\text{eff}}J_x. \end{aligned} \quad (21)$$

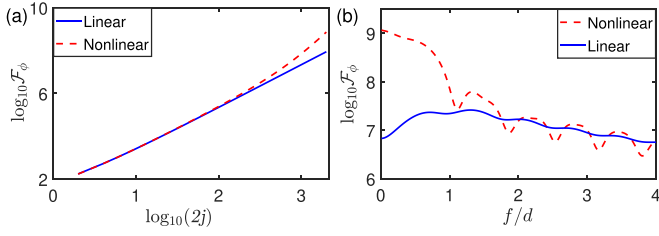


FIG. 2. (a) QFI versus the photon number $2j$, $ft = dt = 10$. (b) QFI versus the parameter f for $j = 500$, $dt = 10$. The parameters are set as $e = 0$ for linear scheme and $e = 0.01d$ for nonlinear scheme.

For a fixed photon number, the first two terms are constant and the Hamiltonian is equivalent to $H = H_0 + H_1$, where H_0 is given by Eq. (15) and

$$H_1 = eJ_z^2 \quad (22)$$

with $e = 2U$.

For the nonlinear system, it is complicated to compute the QFI directly. However, considering a weak nonlinear effect $e \ll d$, we keep to the first order of e and the results yield $\mathcal{H}_{\text{non}} = \mathcal{H}_0 + \mathcal{H}_1$, where \mathcal{H}_0 is given by Eq. (17) and

$$\mathcal{H}_1 = \sum_{\alpha, \beta \neq \alpha} C_{\alpha\beta} \{J_\alpha, J_\beta\} + C_{xx}(J_x^2 - J_y^2) + C_{yy}(J_y^2 - J_z^2) \quad (23)$$

and $\alpha, \beta = x, y, z$, $\{J_\alpha, J_\beta\} = J_\alpha J_\beta + J_\beta J_\alpha$, $C_{\alpha\beta}$, C_{xx} , and C_{yy} are given in Appendix C.

The analytical results of the QFI are still tedious, so we only give the numerical results here. The linear and nonlinear contributions lead to a competition of the terms of QFI with different dependence on the total photon number. In Fig. 2(a), we compare the QFI as functions of the photon number between linear ($e = 0$) and nonlinear ($e \neq 0$) setups. The difference between the red dashed and blue solid lines demonstrates the nonlinear effect. The results show that the nonlinear effect plays a leading role on QFI when the photon number is large enough. In general, the nonlinear effect is beneficial to break the Heisenberg limit [47–49]. Since the complete expression of QFI [with \mathcal{H} being given by Eq. (23)] is too tedious, in Appendix C we only give one term in the results by Eq. (C8), which achieves that scales as n^3 , being much better than the Heisenberg limit n^2 even within a low nonlinear effect. Furthermore, while $d = 0$, the QFI will degrade into $\mathcal{F} = (\partial f / \partial \Delta) t^2$, which is consistent with the linear one. In addition, in Fig. 2(b), we plot the QFI as a function of the parameter f on a log-log scale for the linear and nonlinear scheme. It can be observed clearly that the nonlinear curve is much larger than the linear one for $f \lesssim d$. However, for $f \gtrsim d$, it becomes choppy in the linear region.

In fact, the distribution of the state has exerted a decisive effect in the above metrology process. As an illustration, we plot the function $|\langle j, m | \psi(t) \rangle|^2$ versus m in Fig. 3. For $j = 100$, in Figs. 3(a) and 3(b), we plot $|\langle j, m | \psi(t) \rangle|^2$ for linear and nonlinear scheme, respectively. It shows that the distribution for the nonlinear scheme is radically different

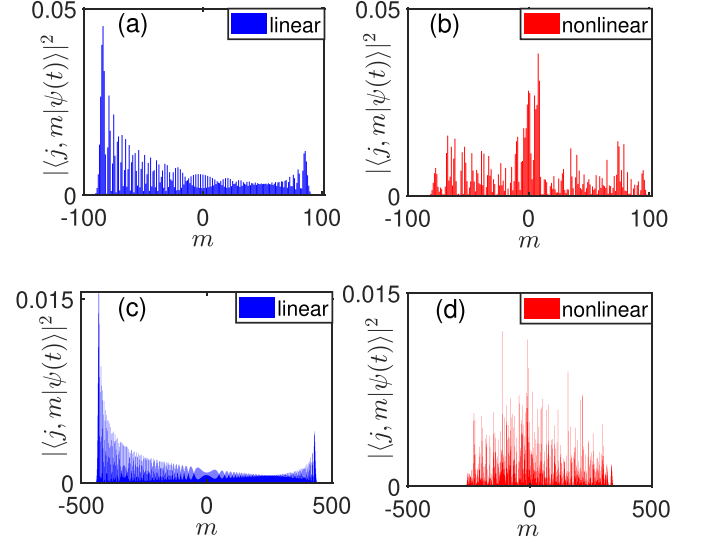


FIG. 3. Distribution of $|\langle j, m | \psi(t) \rangle|^2$ versus m for (a,c) linear scheme and (b,d) nonlinear scheme. For (a) and (b), the parameters are set as $j = 100$, $ft = dt = 10$, $e = 0$ for (a) and $e = 0.01d$ for (b). For (c) and (d), the parameters are set as $j = 500$, $ft = dt = 10$, $e = 0$ for (c) and $e = 0.01d$ for (d).

from the linear one, however, their distribution ranges are approximately the same. For $j = 500$, analogously to Figs. 3(c) and 3(d), the function $|\langle j, m | \psi(t) \rangle|^2$ versus m is plotted. It is obvious that the distribution for the nonlinear scheme [Fig. 3(d)] is more compressed than the one for the linear scheme [Fig. 3(c)]. Recall that we showed in Fig. 2(a), the linear QFI and the nonlinear QFI are almost unanimous for $j = 100$, however, the nonlinear QFI is much larger than the linear one for $j = 500$. Therefore, the nonlinearity can induce the compressibility of state distribution, thereby enhancing the QFI of system. The state distribution can be also illustrated by the Husimi Q function, which represents the anisotropic quasiprobability distribution in a spherical phase space. The Q function is defined as [50,51]

$$Q(\theta_0, \phi_0) = \frac{1}{\pi} \langle \theta_0, \phi_0 | \rho | \theta_0, \phi_0 \rangle, \quad (24)$$

where $|\theta_0, \phi_0\rangle$ is the coherent spin state

$$|\theta_0, \phi_0\rangle = \exp\{i\theta_0[J_x \sin(\phi_0) - J_y \cos(\phi_0)]\} |j, -j\rangle \quad (25)$$

and ρ is the density matrix of the considered system. In Figs. 4(a) and 4(b), we plot Q functions for the linear and nonlinear schemes, respectively. Compared with the linear scheme, the central area for the nonlinear one [here the nonlinearity strength is 20 times larger than that in Figs. 3(b) and 3(d)] becomes much smaller. Combining the scale of the color bar, we can see that the Q function distribution becomes more uniform for the nonlinear setup. Meanwhile, we plot $|\langle j, m | \psi(t) \rangle|^2$ versus m under the same condition (the few number of photons and the relatively big nonlinear effect) in Figs. 4(c) and 4(d). In this case, the compressibility of the state distribution for the nonlinear scheme is revealed again.

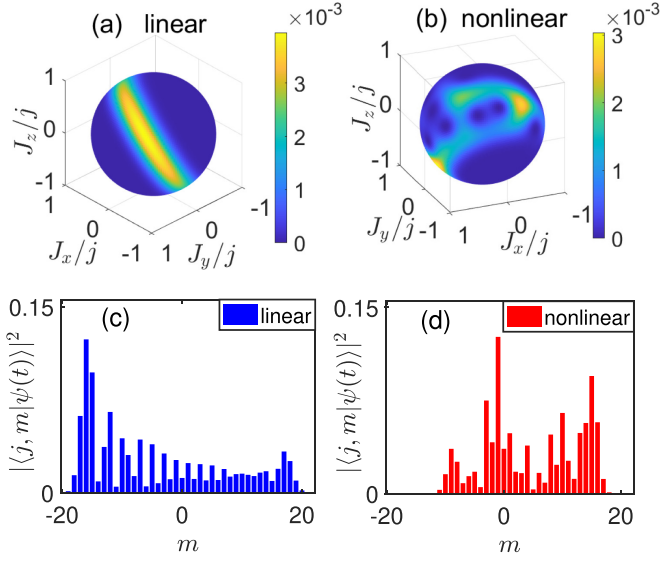


FIG. 4. (a,b) Q function versus the angles θ_0 and ϕ_0 for linear scheme and nonlinear scheme, respectively. The parameters are set as $j = 20$, $ft = dt = 10$, $e = 0$ for (a) and $e = 0.2d$ for (b). (c,d) Distribution of $|\langle j, m | \psi(t) \rangle|^2$ versus m for linear scheme and nonlinear scheme, respectively. The parameters are same as set as $j = 20$, $ft = dt = 10$, $e = 0$ for (c) and $e = 0.2d$ for (d).

IV. CONCLUSION

In conclusion, with reference to the traditional SU(2) interferometer model, we implement a similar algebraic setup for the rotation sensing in a microcavity. In our scheme, we employ a detuning two-level atom to create the effective coupling between two optical modes, thanks to which the initial state is extended to the entire Hilbert space during the time evolution. We find that the accuracy of the parameter estimation can be enhanced dramatically by the coupling, via encoding the estimated angular velocity into both of the amplitudes and the phase of the wave function. Moreover, we study the nonlinear system which can be described by the Bose-Hubbard model and find that the accuracy of the parameter estimation can even break the Heisenberg limit with the large photon number. This enhancement is associated with the compressibility of the state distribution.

Our study suggests some viable strategies that may be used to benefit the enhancement of the rotating sensing which include the following: use a largely detuned atom to induce the coupling between two optical modes; introduce some nonlinear interaction in the system; rotate the system with a certain angular velocity. We hope that our metrology scheme with the assistance of detuning particle can be useful for the designing of quantum gyroscope based on the Sagnac effect.

ACKNOWLEDGMENTS

We thank Prof. X.-M. Lu for useful discussions. This work is supported by National Key R&D Program of China (Grant No. 2021YFE0193500), by National Natural Science Foundation of China (Grants No. 11875011, No. 12047566, No. 11875231, and No. 11935012).

APPENDIX A: FRÖLICH-NAKAJIMA TRANSFORMATION

For our model of the WGM optical microresonator which couples to a two-level detuning atom, the Hamiltonian can be described by Eqs. (13) and (14) in the main text. The rotating-wave approximation demands that the coupling strength and detuning satisfy, respectively, $g_\gamma \ll \{\omega_\gamma, \omega_a\}$ and $|\Delta_\gamma| \ll \{\omega_\gamma, \omega_a\}$, where $\Delta_\gamma = \omega_a - \omega_\gamma$.

To proceed, we assume $g_\gamma \ll \Delta_\gamma$, the effective coupling between two cavity modes are obtained by the Frölich-Nakajima transformation [52–54], which is widely used in condensed-matter physics and quantum optics. By eliminating the degree of freedom of the atom, a weak coupling will be established between the two modes. In what follows, we will give the detailed derivations for the transformation.

At first, we introduce a unitary transformation $\tilde{H} = \exp(-\lambda S)H \exp(\lambda S)$, which can be expanded via Taylor expansions

$$\begin{aligned} \tilde{H} &\approx H_0 + \lambda(H_I + [H_0, S]) \\ &+ \lambda^2([H_I, S] + [[S, [S, H_0]]) + O(\lambda), \end{aligned} \quad (\text{A1})$$

where λ is introduced to mark the order of perturbation and would be set to 1 after all calculations. S is an anti-Hermitian operator. Then, setting the first-order perturbation term $H_I + [H_0, S] = 0$, we obtain

$$S = g_{cw}a_{cw}|e\rangle\langle g| + g_{ccw}a_{ccw}|e\rangle\langle g| - \text{H.c.} \quad (\text{A2})$$

Considering the dispersive interaction between the atom and resonator modes, we approximate that the atom prepared in initial state $|g\rangle$ will always be in the ground state $|g\rangle$. Neglecting the high-frequency terms, the effective Hamiltonian satisfies

$$\tilde{H} = H_{\text{eff}} \otimes |g\rangle\langle g|. \quad (\text{A3})$$

At last, up to second-order interactions, our effective Hamiltonian is obtained as $H_{\text{eff}} = H_{\text{eff},\omega} + H_{\text{eff},I}$, where

$$H_{\text{eff},\omega} = \sum_{\gamma} \left(\omega_{\gamma} + \frac{|g_{\gamma}|^2}{\Delta_{\gamma}} \right) a_{\gamma}^{\dagger} a_{\gamma}, \quad (\text{A4})$$

and

$$H_{\text{eff},I} = \sum_{\gamma, \gamma' \neq \gamma} \frac{1}{2} \left(\frac{1}{\Delta_{\gamma}} + \frac{1}{\Delta_{\gamma'}} \right) g_{\gamma} g_{\gamma'} a_{\gamma}^{\dagger} a_{\gamma'}. \quad (\text{A5})$$

We further define

$$g_{\text{eff}} = \frac{1}{2} \left(\frac{1}{\Delta_{cw}} + \frac{1}{\Delta_{ccw}} \right) g_{cw} g_{ccw}, \quad (\text{A6})$$

in the interaction picture and Schwinger representation, the effective Hamiltonian can be reduced

$$\begin{aligned} \tilde{H}_{\text{eff}} &= \exp(iH_{\text{eff},\omega}t) H_{\text{eff},I} \exp(-iH_{\text{eff},\omega}t) \\ &= 2\Delta J_z + 2g_{\text{eff}} J_x, \end{aligned} \quad (\text{A7})$$

which is Eq. (15) in the main text.

To verify the above approach, we respectively employ the exact Hamiltonian [see Eqs. (13) and (14)] and the approximate Hamiltonian \tilde{H}_{eff} to illustrate the dynamics of the system. Choosing the initial state as $|in\rangle = (|n, n, g\rangle + |n +$

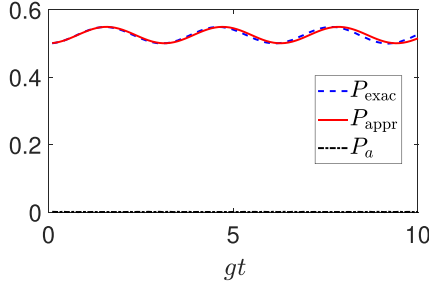


FIG. 5. Dynamics of the system which is governed by the exact and approximate Hamiltonian. The parameters are set as $n = 20$, $\Delta = g$, $\omega_l = 1600g$, $\omega_a = 2000g$, and $g_{\text{eff}} = g^2/(\omega_a - \omega_l)$.

$1, n-1, g\rangle/\sqrt{2}$ and $|\text{in}\rangle = (|n, n\rangle + |n+1, n-1\rangle)/\sqrt{2}$ for exact and approximate approaches respectively. We compare the dynamics of the system in Fig. 5. Here, we plot the dynamics of $P_{\text{exact}} = |\langle n, n | \psi_{\text{exact}}(t) \rangle|^2$ (the blue dotted line) and the detuning atom $P_a = |\langle e | \psi_{\text{exact}}(t) \rangle|^2$ (the black dotted line) for the exact solution. Moreover, for the approximate solution, we plot the dynamics of $P_{\text{appr}} = |\langle n, n | \psi_{\text{appr}}(t) \rangle|^2$ (the red solid line). The agreement between P_{exact} and P_{appr} shows the validity of our approach. The fact $P_a \approx 0$ during the time evolution gives a numerical verification of Eq. (A3).

APPENDIX B: QFI IN DIFFERENT STATES

In the main text, we mentioned that the QFI is enhanced by encoding the parameter Δ into both of the amplitudes and the phase of the wave function. We will give more details in this Appendix. To this end, we now define a general pure state

$$|\psi\rangle = \sum_n a_n \exp(i\varphi_n) |\psi_n\rangle, \quad (\text{B1})$$

where φ_n and a_n are the real phase and the amplitude of the state $|\psi_n\rangle$, respectively, and the normalization condition demands $\sum_n a_n^2 = 1$. To analyze the QFI in a different state, we consider the following two situations.

First, we consider the case that only the phases are dependent on the estimated parameter, that is, $\varphi_n = \varphi_n(\Delta)$. Then the QFI is

$$\mathcal{F}_{1,\Delta} = 4 \left[\sum_n a_n^2 \left(\frac{\partial \varphi_n}{\partial \Delta} \right)^2 - \left| \sum_n a_n^2 \frac{\partial \varphi_n}{\partial \Delta} \right|^2 \right]. \quad (\text{B2})$$

Second, when the phases and the probability amplitudes are both related to Δ , the QFI can be obtained by

$$\mathcal{F}_{2,\Delta} = \mathcal{F}_{1,\Delta} + 4 \sum_n \left(\frac{\partial a_n}{\partial \Delta} \right)^2. \quad (\text{B3})$$

Here, the second term $4 \sum_n \left(\frac{\partial a_n}{\partial \Delta} \right)^2$ is the contribution from the probability amplitudes with parameter Δ . Obviously, encoding the information of Δ into both of the phases and the amplitudes is beneficial for parameter estimation.

APPENDIX C: QFI FOR NONLINEAR EFFECT

In the Eq. (23) of the main text, we obtained the formal solution of the Hermitian operator \mathcal{H} . Here, we give the concrete

expression and derivation process through the Baker-Hausdorff formula [43,44,55]

$$\mathcal{H} = -t \frac{\partial H}{\partial \Delta} + i \sum_{n=1}^{\infty} \frac{(it)^{n+1}}{(n+1)!} H^{\times n} \frac{\partial H}{\partial \Delta}, \quad (\text{C1})$$

where the super operator $H^{\times n}$ denotes an n th-order nested commutator operation, $H^{\times}(\cdot) = [H, \cdot]$. Then we have

$$\begin{aligned} \mathcal{H} = & C_x J_x + C_y J_y + C_z J_z + C_{xx} (J_x^2 - J_y^2) \\ & + C_{yy} (J_y^2 - J_z^2) + C_{xy} (J_x J_y + J_y J_x) \\ & + C_{yz} (J_y J_z + J_z J_y) + C_{zx} (J_z J_x + J_x J_z), \end{aligned} \quad (\text{C2})$$

where

$$\begin{aligned} C_{xy} = & -\frac{e}{6f^2} \frac{\partial f}{\partial \Delta} \left\{ \frac{2A_1}{r^2} [\cos(rt) - 1] \right. \\ & - \frac{A_1 - B_1/\eta}{\Lambda_1^2} [\cos(\Lambda_1 t) - 1] \\ & \left. - \frac{A_1 + B_1/\eta}{\Lambda_2^2} [\cos(\Lambda_2 t) - 1] \right\}, \end{aligned} \quad (\text{C3})$$

$$\begin{aligned} C_{yz} = & \frac{e}{3fd} \frac{\partial f}{\partial \Delta} \left\{ \frac{A_2}{r^2} [\cos(rt) - 1] \right. \\ & - \frac{A_2 + B_2/\eta}{2\Lambda_1^3} [\cos(\Lambda_1 t) - 1] \\ & \left. - \frac{A_2 - B_2/\eta}{2\Lambda_2^3} [\cos(\Lambda_2 t) - 1] \right\}, \end{aligned} \quad (\text{C4})$$

$$\begin{aligned} C_{zx} = & \frac{e}{3f^2 d} \frac{\partial f}{\partial \Delta} \left\{ \frac{A_3 + f^2 d^2}{r^3} [\sin(rt) - rt] \right. \\ & - \frac{A_3 + B_3/\eta}{2\Lambda_1^3} [\sin(\Lambda_1 t) - \Lambda_1 t] \\ & \left. - \frac{A_3 - B_3/\eta}{2\Lambda_2^3} [\sin(\Lambda_2 t) - \Lambda_2 t] \right\}, \end{aligned} \quad (\text{C5})$$

$$\begin{aligned} C_{xx} = & -\frac{e}{6f} \frac{\partial f}{\partial \Delta} \left\{ \frac{2A_1}{r^3} [\sin(rt) - rt] \right. \\ & - \frac{A_1 - B_1/\eta}{\Lambda_1^3} [\sin(\Lambda_1 t) - \Lambda_1 t] \\ & \left. - \frac{A_1 + B_1/\eta}{\Lambda_2^3} [\sin(\Lambda_2 t) - \Lambda_2 t] \right\}, \end{aligned} \quad (\text{C6})$$

and

$$\begin{aligned} C_{yy} = & \frac{e}{3f} \frac{\partial f}{\partial \Delta} \left\{ \frac{2A_2}{r^3} [\sin(rt) - rt] \right. \\ & - \frac{A_2 + B_2/\eta}{\Lambda_1^3} [\sin(\Lambda_1 t) - \Lambda_1 t] \\ & \left. - \frac{A_2 - B_2/\eta}{\Lambda_2^3} [\sin(\Lambda_2 t) - \Lambda_2 t] \right\}, \end{aligned} \quad (\text{C7})$$

where $\Lambda_1 = [(3f^2 + 3d^2 - \eta)/2]^{1/2}$, $\Lambda_2 = [(3f^2 + 3d^2 + \eta)/2]^{1/2}$, $\eta = [f^4 + d^4 + 14f^2 d^2]^{1/2}$, and

$$\begin{aligned} A_1 = & d^2 - 4f^2, & B_1 = & (f^2 - d^2)(4f^2 + d^2), \\ A_2 = & f^2 - d^2, & B_2 = & f^4 - d^4 + 6f^2 d^2, \\ A_3 = & 2f^4 + d^4 - 6f^2 d^2, & B_3 = & 2f^6 + d^6 + 8f^4 d^2 + f^2 d^4. \end{aligned}$$

The complete expression for the QFI $\mathcal{F}_\Delta = 4(\langle \mathcal{H}^2 \rangle - \langle \mathcal{H} \rangle^2)$ [with \mathcal{H} being given by Eq. (23)] possesses 36 terms, which is too tedious to be given term by term here. However, we note that $\{C_{xx}, C_{yy}, C_{xy}, C_{yz}, C_{zx}\} \propto e^1$ and $\{C_x, C_y, C_z\} \propto e^0$. Therefore, in the expression of the QFI, six terms are proportional to e^0 , 15 terms are proportional to e^1 while the remaining 15 terms are proportional to e^2 . The first six terms in the order of e^0 are exactly the QFI without the nonlinear interaction, which is given by Eq. (19) in the main text. The last

15 terms in the order of e^2 can be neglected in the situation of small e . Now, we give one typical term which is proportional to e^1 , for example,

$$C_x C_{xx} \{ \langle J_x (J_x^2 - J_y^2) + (J_x^2 - J_y^2) J_x \rangle - 2 \langle J_x \rangle \langle J_x^2 - J_y^2 \rangle \} \\ \propto \frac{1}{8} C_x C_{xx} [(j-1)(j+2)\sqrt{j(j+1)}]. \quad (C8)$$

Since $j = n/2$, it shows that we here achieve a n^3 scaling for the QFI, which is beyond the Heisenberg limit.

-
- [1] C. M. Caves, *Phys. Rev. Lett.* **45**, 75 (1980).
 - [2] C. M. Caves, *Phys. Rev. D* **23**, 1693 (1981).
 - [3] V. Giovannetti, S. Lloyd, and L. Maccone, *Science* **306**, 1330 (2004).
 - [4] V. Giovannetti, S. Lloyd, and L. Maccone, *Phys. Rev. Lett.* **96**, 010401 (2006).
 - [5] D. W. Berry, B. L. Higgins, S. D. Bartlett, M. W. Mitchell, G. J. Pryde, and H. M. Wiseman, *Phys. Rev. A* **80**, 052114 (2009).
 - [6] J. Joo, W. J. Munro, and T. P. Spiller, *Phys. Rev. Lett.* **107**, 083601 (2011).
 - [7] H. S. Eisenberg, J. F. Hodelin, G. Khoury, and D. Bouwmeester, *Phys. Rev. Lett.* **94**, 090502 (2005).
 - [8] I. Afek, O. Amber, and Y. Silberberg, *Science* **328**, 879 (2010).
 - [9] K. J. Resch, K. L. Pregnell, R. Prevedel, A. Gilchrist, and G. J. Pryde, J. L. O'Brien, and A. G. White, *Phys. Rev. Lett.* **98**, 223601 (2007).
 - [10] D. Leibfried, M. D. Barrett, T. Schaetz, J. Britton, J. Chiaverini, W. M. Itano, J. D. Jost, C. Langer, and D. J. Wineland, *Science* **304**, 1476 (2004).
 - [11] K. X. Sun, M. M. Fejer, E. Gustafson, and R. L. Byer, *Phys. Rev. Lett.* **76**, 3053 (1996).
 - [12] A. N. Boto, P. Kok, D. S. Abrams, S. L. Braunstein, C. P. Williams, and J. P. Dowling, *Phys. Rev. Lett.* **85**, 2733 (2000).
 - [13] S. J. Bentley and R. W. Boyd, *Opt. Express* **12**, 5735 (2004).
 - [14] S. H. Tan, B. I. Erkmen, V. Giovannetti, S. Guha, S. Lloyd, L. Maccone, S. Pirandola, and J. H. Shapiro, *Phys. Rev. Lett.* **101**, 253601 (2008).
 - [15] V. Giovannetti, S. Lloyd, L. Maccone, and J. H. Shapiro, *Phys. Rev. A* **79**, 013827 (2009).
 - [16] M. Tsang, J. H. Shapiro, and S. Lloyd, *Phys. Rev. A* **78**, 053820 (2008).
 - [17] S. Lloyd, *Science* **321**, 1463 (2008).
 - [18] G. Khoury, H. S. Eisenberg, E. J. S. Fonseca, and D. Bouwmeester, *Phys. Rev. Lett.* **96**, 203601 (2007).
 - [19] S. D. Huver, C. F. Wildfeuer, and J. P. Dowling, *Phys. Rev. A* **78**, 063828 (2008).
 - [20] B. Yurke, S. L. McCall, and J. R. Klauder, *Phys. Rev. A* **33**, 4033 (1986).
 - [21] M. Kasevich and S. Chu, *Phys. Rev. Lett.* **69**, 1741 (1992).
 - [22] C. E. Wieman, D. E. Pritchard, and D. J. Wineland, *Rev. Mod. Phys.* **71**, S253 (1999).
 - [23] X. M. Lu, H. Krovi, R. Nair, S. Guha, and J. H. Shapiro, *npj Quantum Inf.* **4**, 64 (2018).
 - [24] N. Fang, H. Lee, C. Sun, and X. Zhang, *Science* **308**, 534 (2006).
 - [25] J. G. Fujimoto, M. E. Brezinski, G. J. Tearney, S. A. Boppart, B. Bouma, M. R. Hee, J. F. Southern, and E. A. Swanson, *Nature Medicine* **1**, 970 (1995).
 - [26] Y. Martin, D. W. Abraham, and H. K. Wickramasinghe, *Appl. Phys. Lett.* **52**, 1103 (1988).
 - [27] F. Jelezko and J. Wrachtrup, *Phys. Status Solidi A* **203**, 3207 (2006).
 - [28] M. W. Doherty, V. V. Struzhkin, D. A. Simpson, L. P. McGuinness, Y. Meng, A. Stacey, T. J. Karle, R. J. Hemley, N. B. Manson, L. C. L. Hollenberg, and S. Prawer, *Phys. Rev. Lett.* **112**, 047601 (2014).
 - [29] L. Rondin, J. P. Tetienne, T. Hingant, J. F. Roch, P. Maletinsky, and V. Jacques, *Rep. Prog. Phys.* **77**, 056503 (2014).
 - [30] G. Balasubramanian, P. Neumann, D. Twitchen, M. Markham, R. Kolesov, N. Mizuochi, J. Isoya, J. Achard, J. Beck, J. Tissler, V. Jacques, P. R. Hemmer, F. Jelezko, and J. Wrachtrup, *Nat. Mater.* **8**, 383 (2009).
 - [31] T. Wolf, P. Neumann, K. Nakamura, H. Sumiya, T. Ohshima, J. Isoya, and J. Wrachtrup, *Phys. Rev. X* **5**, 041001 (2015).
 - [32] K. U. Schreiber and J.-P. R. Wells, *Rev. Sci. Instrum.* **84**, 041101 (2013).
 - [33] A. D. V. Di Virgilio, A. Basti, N. Beverini, F. Bosi, G. Carelli, D. Ciampini, F. Fuso, U. Giacomelli, E. Maccioni, P. Marsili, A. Ortolan, A. Porzio, A. Simonelli, and G. Terreni, *Phys. Rev. Research* **2**, 032069(R) (2020).
 - [34] J. Ahn, Z. Xu, J. Bang, Y.-H. Deng, T. M. Hoang, Q. Han, R.-M. Ma, and T. Li, *Phys. Rev. Lett.* **121**, 033603 (2018).
 - [35] R. Reimann, M. Doderer, E. Hebestreit, R. Diehl, M. Frimmer, D. Windey, F. Tebbenjohanns, and L. Novotny, *Phys. Rev. Lett.* **121**, 033602 (2018).
 - [36] S. L. Braunstein and C. M. Caves, *Phys. Rev. Lett.* **72**, 3439 (1994).
 - [37] S. L. Braunstein, C. M. Caves, and G. J. Milburn, *Ann. Phys. (NY)* **247**, 135 (1996).
 - [38] W. W. Chow, J. Gea-Banacloche, L. M. Pedrotti, V. E. Sanders, W. Schleich, and M. O. Scully, *Rev. Mod. Phys.* **57**, 61 (1985).
 - [39] J. Li, M. G. Suh, and K. Vahala, *Optica* **4**, 346 (2017).
 - [40] M. N. Armenise, C. Ciminelli, F. Dell'Olivo, and V. M. M. Passaro, *Advances in Gyroscope Technologies* (Springer, New York, 2010).
 - [41] S. Maayani, R. Dahan, Y. Kligerman, E. Moses, A. U. Hassan, H. Jing, F. Nori, D. N. Christodoulides, and T. Carmon, *Nature (London)* **558**, 569 (2018).
 - [42] G. B. Malykin, *Phys. Usp.* **43**, 1229 (2000).
 - [43] X. X. Jing, J. Liu, H. N. Xiong, and X. G. Wang, *Phys. Rev. A* **92**, 012312 (2015).

- [44] J. Liu, X. X. Jing, and X. G. Wang, *Sci. Rep.* **5**, 8565 (2014).
- [45] M. J. Hartmann, F. G. S. L. Brandão, and M. B. Plenio, *Laser & Photons. Rev.* **2**, 527 (2008).
- [46] M. J. Hatmann, F. G. S. L. Brandão, and M. B. Plenio, *New J. Phys.* **10**, 033011 (2008).
- [47] L. Pezze and A. Smerzi, *Phys. Rev. Lett.* **102**, 100401 (2009).
- [48] J. Beltran and A. Luis, *Phys. Rev. A* **72**, 045801 (2005).
- [49] A. Luis, *Phys. Lett. A* **329**, 8 (2005).
- [50] A. Widera, S. Trotzky, P. Cheinet, S. Folling, F. Gerbier, I. Bloch, V. Gritsev, M. D. Lukin, and E. Demler, *Phys. Rev. Lett.* **100**, 140401 (2008).
- [51] J. M. Radcliffe, *J. Phys. A* **4**, 313 (1971).
- [52] H. B. Zhu and C. P. Sun, *Chin. Sci. A* **30**, 928 (2000); *Prog. Chin. Sci.* **10**, 698 (2000).
- [53] Y. Li, C. Bruder, and C. P. Sun, *Phys. Rev. A* **75**, 032302 (2007).
- [54] M. Boissonneault, J. M. Gambetta, and A. Blais, *Phys. Rev. A* **79**, 013819 (2009).
- [55] S. S. Pang and T. A. Brun, *Phys. Rev. A* **90**, 022117 (2014).